Comparing the Lithiation and Sodiation of a Hard Carbon Anode Using In Situ Impedance Spectroscopy

Fabian Linsenmann,*,z Daniel Pritzl, and Hubert A. Gasteiger**

Chair of Technical Electrochemistry, Department of Chemistry and Catalysis Research Center, Technische Universität München, 85748 Garching, Germany

We present *in situ* electrochemical impedance spectroscopy data measured during (de)sodiation and (de)lithiation of a commercial hard carbon (HC) anode material. For this purpose, two different systems of *micro*-reference electrodes (μ-RE) were used: a gold-wire reference electrode (μ-GWRE) for Li/HC half-cells and a tin-wire reference electrode (μ-TWRE) for Na/HC half-cells. We show that for both (de)sodiation (using EC/DMC + 1 M NaPF$_6$ electrolyte) and (de)lithiation (using EC/EMC + 1 M LiPF$_6$ electrolyte) the impedance spectra are dominated by a charge transfer resistance (R_{CT}) which is reversibly decreasing/increasing with increasing/decreasing state-of-charge. The contributions to the HC electrode resistance (R_{anode}), i.e., charge transfer (R_{CT}), pore (R_{pore}), and separator resistance (R_{HFR}), were obtained by fitting the impedance spectra using a representative equivalent circuit. We conclude that the R_{CT} associated with sodiation of HC is ≈10-fold higher compared to the lithiation of HC at 100% SOC. Furthermore, we compare the evolution of R_{anode} measured *in situ* over 52 cycles at the same SOC. We find that the higher electrode resistances for sodiated HC result in a considerably reduced rate capability for HC sodiation. For a potential future commercialization of sodium-ion batteries, the fast-charging properties (=HC sodiation) would be a crucial performance indicator.

Until today, graphite is the almost exclusively used anode active material (AAM) in commercial lithium-ion batteries (LIBs) owing to its high capacity (≈350–360 mAh/g$_{graphite}$) and low average discharge potential,[1,2] resulting in a relatively high energy density. In 2016, the market share of anode active materials for commercial LIBs was 89% graphite (43% artificial and 46% natural graphite), 7% amorphous carbon, 2% lithium titanate (LTO) and 2% silicon or tin-based materials.[3] Interestingly, the very first LIB introduced by Sony in 1991 used an amorphous (disordered) carbon anode, more precisely a soft carbon (SC) with a specific capacity of ≈220 mAh/g$_{SC}$.[4,5] This cell with an LiCoO$_2$ cathode yielded an energy density of ≈80 Wh kg^{-1},[4,5] considerably more than the back then used nickel-cadmium cells (≈50 Wh kg^{-1}).[6] Two classes of amorphous carbons are typically distinguished: hard carbons (HC) that exhibit a high degree of cross-linking between graphitic domains and therefore cannot be graphitized even at very high temperatures, and soft carbons with little cross-linking where neighboring graphitic domains have a tendency to lie in almost parallel pre-orientation, so that they can be transformed into the graphitic state by pyrolysis at temperatures between 2000 °C–3000 °C.[7] The SC anode in Sony's first generation LIB was substituted already one year later by a HC anode with a higher capacity of ≈320 mAh/g$_{HC}$, resulting in an energy density of ≈120 Wh kg^{-1} with a LiCoO$_2$ cathode.[4] While graphite is known to undergo a volume expansion of ≈10% during lithium intercalation,[8] with the d-spacing between neighboring graphene layers increasing from 0.335 to ≈0.37 nm,[9] HCs typically show higher d-spacings already in their delithiated state (>0.38 nm), so that they, contrary to graphite, do not undergo volume expansion upon lithiation.[4,5] Nishi et al.[4,5] explain the very high full-cell cycling stability of HC based LIBs by the absence of volume change upon lithiation/delithiation, which is supposed to decrease lithium inventory losses induced by cracking of the solid electrolyte interphase (SEI) caused by volume changes, a well-known aging mechanism of graphite anodes during long-term cycling, especially at elevated temperatures.[10,11] However, the lower density of HCs[7,12] (≈1.45–1.55 g cm^{-3} vs 2.2 g cm^{-3} for graphite) and their relatively high first-cycle irreversible capacity losses of ≈20%[4,5,13] (vs <10%

for graphite[14,15]) significantly reduce the energy density of the cell. Therefore, the development of new electrolytes based on ethylene carbonate[16] that enabled the application of graphite as anode active material, gradually led to the replacement of HC anodes by graphite in LIBs.[5] Furthermore, the fact that the graphite potential for lithium (de) intercalation is close to that of metallic lithium (≈100 mV vs Li$^+$/Li) over nearly the entire charge/discharge curve increases the energy density compared to HCs that typically feature sloping voltage profiles.[17] Consequently, while in 1997 the market shares of HC and graphite were still 52% and 43%,[18] respectively, today artificial and natural graphites are dominating the anode material market, as mentioned above.[2,3]

In the literature, it is often argued that some HCs can incorporate lithium-ions in ratios higher than the well-known LiC$_6$ stoichiometry found for fully intercalated graphite,[1] which should allow for practical reversible capacities above the theoretical capacity of graphite of 372 mAh/g$_{graphite}$. In fact, high reversible capacities for lithium insertion into HCs are reported in the literature.[5,13,19–23] However, since the voltage profiles at higher state-of-charge (SOC) become very flat for HCs, a considerable fraction of their capacity is obtained at potentials significantly below 100 mV vs Li$^+$/Li[13,19] and can typically only be accessed by constant voltage holds at the end of the charging phase at very low potentials of ≈10 mV vs Li$^+$/Li. Additionally, the thus obtained high reversible capacities are often accompanied by high irreversible capacity losses[21] and a large voltage hysteresis.[13] Novak et al.[24] therefore point out that even though some HCs do show reversible capacities above the theoretical specific capacity of graphite, the actually usable capacity is restricted in practical applications. In summary, the main issues related to a commercial use of HCs are[24]: a) the risk of lithium plating at potentials close to 0 V vs Li$^+$/Li at the end of charge, if high lithiation capacities are to be utilized; b) an often observed coulombic efficiency (CE) decrease when charging to such low voltages; and c) the flat potential profile that makes it difficult to properly control the cutoff cell voltage during charging in order to prevent overcharging.

While graphite is now used almost exclusively in LIBs, it cannot be used as anode active material in sodium-ion batteries (SIBs), as it is widely accepted that graphite cannot reversibly intercalate sodium-ions when using standard organic carbonate-based electrolytes.[25] The reason for this is believed to be the thermodynamic instability of the resulting Na-C-phases.[26] On the other

hand, electrochemical sodium insertion reactions into disordered carbons have been observed and reported already in the late 1980s,[27] and probably some of the first experiments on rechargeable sodium-ion cells were published by Doeff et al. in 1993,[28] who demonstrated cycling of a sodium-ion battery consisting of a HC anode (petroleum coke), a solid polymer electrolyte, and a sodium cobalt bronze cathode ($Na_{0.6}CoO_2$). For the petroleum coke, a maximum stoichiometry of NaC_{15} could be obtained, which would correspond to a specific capacity of ≈ 149 mAh/g_{HC}.

The storage mechanism of both lithium and sodium in disordered carbonaceous materials, such as HCs, is still not completely understood and under ongoing discussion in the literature.[29] The first studies where the intercalaction mechanism of lithium and sodium in HCs was investigated and directly compared were reported by Stevens and Dahn in 2000 and 2001.[17,30] These authors conclude from *in situ* wide angle and small angle X-ray scattering (WAXS and SAXS) that the insertion mechanisms for lithium and sodium in HCs seem to be similar. At higher anode potentials (i.e., at low SOCs), the insertion between approximately parallel graphene sheets, described by Liu and Dahn[22] as a "house of cards" structure, was attributed to giving rise to the sloping voltage profile in the low SOC region. Additionally, during the flat, low-voltage plateau found at higher SOC, lithium and sodium fill nanopores in an adsorption-like process occurring at chemical potentials close to that of the metals themselves. Stevens and Dahn could confirm interlayer intercalation at low SOCs also by *in situ* X-ray diffraction (XRD) measurements of the d-spacing increase during lithium or sodium insertion.[17] These results were confirmed by Komaba et al. through *ex situ* XRD and Raman spectroscopy.[31] Evidence for the pore filling mechanism in the high SOC region was obtained from small-angle X-ray spectroscopy (SAXS) data,[17] later on confirmed by Gotoh et al.[32] and Chevallier et al.[33] for lithium via ^7Li solid state NMR and by Stratford et al.[34] and Morita et al.[35] in the case of sodium via ^{23}Na solid state NMR.

In summary, while HC anodes have been replaced by graphite in commercial LIBs, the HC material family is until today still the most promising anode material for SIBs. Therefore, in this study, we want to shed light on the impedance evolution of a commercial HC anode during (de)sodiation in the very first formation cycle and over extended cycling, and compare it with the associated impedance changes in the case of (de)lithiation of the same HC anode material. To the best of our knowledge, SOC-dependent anode impedance data of a HC anode have not been reported in the literature in the case of sodium. As discussed in former studies from our group,[36,37] electrode-specific impedances, i.e., without superposition of the counter electrode (CE) impedance, are only accessible by means of *in situ* impedance measurements using a micro-reference electrode (μ-RE) or via harvesting electrodes and assembling them into symmetrical cells.[38] In this study, we directly compare the evolution of the charge transfer resistance R_{CT} during the first cycle (de)sodiation and (de)lithiation of the same hard carbon active material. We show that the *in situ* obtained impedance spectra collected using μ-REs, namely a micro-tin wire reference electrode (μ-TWRE) in the case of sodium and a micro-gold wire reference electrode (μ-GWRE) in the case of lithium, can be fitted with a simple electrical equivalent circuit to extract R_{CT}, the ionic conduction resistance in the electrolyte phase of the electrode R_{pore}, and the high frequency resistance R_{HFR}. Furthermore, we evaluate the change in anode impedance R_{anode} over the course of 52 cycles and determine the rate capability for sodiation and lithiation of the HC anode, respectively.

Experimental

Electrode and electrolyte preparation.—Hard carbon (HC) electrodes consisted of hard carbon (Kuranode, BET surface area = 5.2 m^2 g^{-1}, Kuraray, Japan), sodium carboxymethyl cellulose (Na-CMC, Sunrose, NPI, Japan), and styrene-butadiene rubber (SBR,

emulsion in water, solid content 40 wt%, Zeon, Japan) at a weight ratio of 97:1.5:1.5. First, Na-CMC was mixed with highly pure water (18 MΩcm, Merck Millipore, Germany) using a planetary mixer (Thinky, USA) at 2000 rpm for 30 min. HC powder was then added in three consecutive steps such as to reach a final solid content of 50 wt% with 2 min mixing in between at 2000 rpm. Finally, SBR was added to the slurry and mixed at 500 rpm for 2 min.

For the electrodes used in Li/HC half-cells, the ink was coated onto copper foil (10 ± 1 μm thickness, MTI, United States) using a 100 μm gap size four-way film applicator (Erichsen, Germany), and then dried at room temperature for 5 h, resulting in electrodes with an average loading of 3.0 ± 0.3 mg_{HC}/cm^2 ($\equiv$0.66 ± 0.07 mAh cm^{-2}, based on a nominal specific capacity of 220 mAh/g_{HC}). Electrodes were punched out at a diameter of 11 mm and dried under dynamic vacuum at 120 °C for 12 h in a glass oven (drying oven 585, Büchi, Switzerland) together with glass fiber separators (diameter = 11 mm, VWR, Germany), and then transferred into an argon-filled glovebox (MBraun, Germany) without exposure to ambient air. The thickness of the as-used uncompressed HC electrodes was 59 ± 2 μm and the porosity was $\approx$60%. The electrolyte consisted of 1 M lithium hexafluorophosphate ($LiPF_6$) in a mixture of ethylene carbonate (EC, ≥99%, Sigma Aldrich) and ethyl methyl carbonate (EMC, BASF SE, Germany) at a weight ratio of 3:7 (LP57, BASF SE, Germany). Lithium disks (diameter = 11 mm, thickness $\approx$450 μm) were punched from commercial lithium foil (99.9%, Albermarle, USA) inside an argon-filled glovebox (O_2 and H_2O < 0.1 ppm).

The electrodes used in Na/HC half-cells were obtained using the same preparation procedure as described above, but casting the HC ink onto aluminum foil (15 ± 1 μm thickness, MTI, United States). The electrode loading was also 3.0 ± 0.3 mg_{HC}/cm^2 ($\equiv$0.84 ± 0.08 mAh cm^{-2}, based on a specific capacity of 280 mAh/g_{HC}). The thickness of the as-used uncompressed HC coating was 59 ± 2 μm and the porosity was $\approx$60%, i.e., identical with the HC electrodes for the Li/HC half-cells. The sodium electrolyte was prepared by mixing 50 vol% ethylene carbonate (EC, ≥99%, Sigma Aldrich) and 50 vol% dimethyl carbonate (DMC, BASF SE, Germany) with 1 M $NaPF_6$ (99.9%, Kishida Chemicals, Japan). Sodium disks (diameter = 11 mm, thickness $\approx$500 μm) were punched out from a sodium foil that was prepared from sodium ingots (99.95%, Sigma Aldrich) inside an argon-filled glovebox (O_2 and H_2O < 0.1 ppm).

A conductivity meter (LF 1100+, SI Analytics, Germany, with a custom made ground-glass fitting) with a built-in temperature sensor was used to measure the conductivity of the used electrolytes at 25 °C.

Assembly and cycling of cells for impedance measurements.—For electrochemical impedance spectroscopy (EIS) measurements, three-electrode Swagelok® T-cells were assembled inside an argon-filled glovebox with a hard carbon working electrode (WE), a lithium or sodium metal counter electrode (CE), and a micro-reference electrode (μ-RE) sandwiched between glass fiber separators; the specially designed connection for μ-REs was described in detail by Solchenbach et al.[36] The cell setup is depicted in Fig. 1a. For the Li/HC half-cells, four glass fiber separators and 120 μl electrolyte were used, whereas two glass fiber separators and 60 μl electrolyte were used for the Na/HC half-cells; the lithium and sodium electrolytes were composed as specified above. Note that the number of separators employed only influences the magnitude of the high-frequency resistance (R_{HFR}) and does not impact the cell performance of the cells reported in this study. In the case of Li/HC half-cells, the μ-RE was a Kapton®-coated μ-gold-wire reference electrode (μ-GWRE) with an overall diameter of 64 μm, as described earlier.[36] In the case of Na/HC half-cells, a sodiated tinned copper wire (diameter = 50 μm, Eurowire Ltd., United Kingdom) with a polyurethane insulation (resulting in a total diameter of $\approx$100 μm) was used as reference electrode (μ-TWRE); preparation and setup were described in detail by Linsenmann et al.[37] The μ-GWRE cannot be employed in SIB cells because the kinetics for lithium-gold alloy formation are too sluggish to allow for an in situ
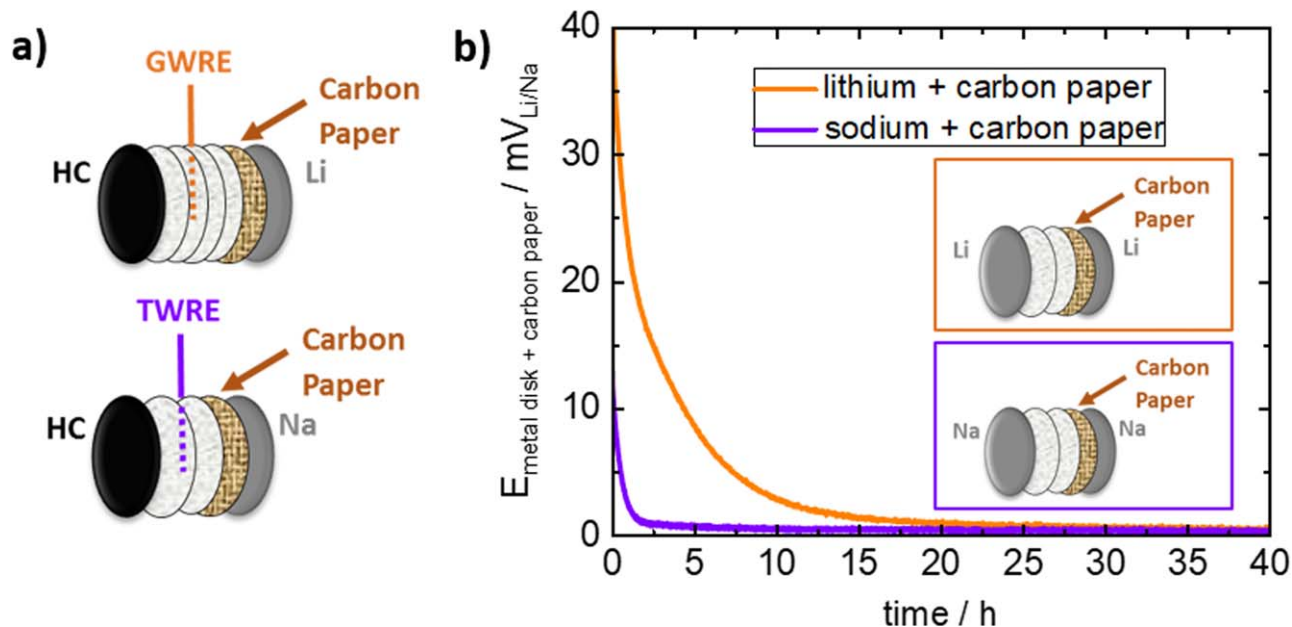
Figure 1. (a) Electrode stack configuration for the *in situ* EIS measurements of a hard carbon (HC) electrode in a Li/HC half-cell with a μ-GWRE (upper sketch) and in a Na/HC half-cell with a μ-TWRE (lower sketch), assembled in three-electrode Swagelok® T-cells.[36] The μ-RE is located centrally between four or two glass fiber separators. A porous carbon paper free-standing electrode is attached to the lithium/sodium metal CE in order to decrease the CE impedance, which is required to obtain artefact-free EIS data. (b) Open circuit voltage (OCV) of the carbon paper + lithium electrode (orange line) or of the carbon paper + sodium electrode (purple line) vs a metallic lithium or sodium CE, respectively. The cell setup is shown in the insets of Fig. 1b.

lithiation of the high-impedance gold wire (diameter only $\approx$50 μm) in a LIB cell, which would be necessary to obtain a stable wire potential allowing for artefact-free EIS measurements.

Unfortunately, recording EIS data with capacitively strongly imbalanced electrodes (i.e., in this case, a high capacity hard carbon WE with low impedance and a low capacity lithium or sodium metal CE with high impedance) leads to artefacts when using a high-impedance μ-RE, as demonstrated recently by Morasch et al.[39] However, attaching a free-standing high-surface area carbon electrode to a metal electrode reduces its impedance, thereby enabling artefact-free half-cell EIS data acquisition.[37,39] Thus, we sandwiched a high-surface area carbon fiber paper (H1410 type from Freudenberg, Germany), cut to 10 mm diameter (150 μm thickness and BET area of $\approx$14 m^2 g^{-1}), between the separator and the metal CE (s. Fig. 1a), thereby reducing the impedance of the latter by means of the gradually occurring chemical lithiation or sodiation of the carbon matrix. In order to determine the mixed potential of the resulting metal/carbon paper composite CE, Swagelok® T-cells were assembled with a metal/carbon paper composite WE, two glass fiber separators, and a metal CE (s. insets in Fig. 1b). Tracking the open circuit voltage (OCV) of these cells reveals that the mixed potential of the metal/carbon paper composite electrode approaches the reversible potential of the pure metal (within <0.5 mV) after $\approx$25 h in the case of lithium and after $\approx$5 h in case of sodium (s. Fig. 1b).

Prior to cell cycling, the μ-REs were sodiated/lithiated *in situ*. This was done by applying a lithiation current of 150 nA for 1[40] in the case of Na/HC half-cells, a constant sodiation current of 50 nA was applied to the μ-TWRE until a potential +10 mV vs the sodium CE was reached.[37] For the SOC-dependent EIS measurements, the Li/HC and the Na/HC half-cells were cycled galvanostatically. The C-rate was C/10 (based on a hard carbon capacity of 280 mAh/g_{HC} for (de)sodiation and of 220 mAh/g_{HC} for (de)lithiation) and cycling was done within a cell potential range of +1.5 V_{cell} and +10 mV_{cell} using a VMP3 potentiostat (Biologic, France). Prior to the EIS measurements, the cell was cycled to different cell potentials (750, 400, 200, 100, 50, and 10 mV_{cell} during lithiation/sodiation as well as 100, 400, and 1500 mV_{cell} during delithiation/desodiation), followed by a 30 min relaxation phase at OCV. Subsequently, potential-controlled electrochemical impedance spectroscopy (PEIS) was

recorded, controlling the voltage perturbation vs the μ-GWRE or the μ-TWRE. The perturbation amplitude was 20 mV and the frequency range 30 kHz–0.1 Hz. All experiments were performed in temperature-controlled chambers (Binder, Germany) at 25 °C.

Assembly and cycling of Li/HC and Na/HC half-cells for rate testing.—Rate-tests for the HC electrodes (3.0 ± 0.3 mg$_{HC}$/cm^2) were performed in conventional three-electrode Swagelok® T-cells with a lithium or sodium metal CE and with a lithium or sodium metal RE, respectively, using four glass fiber separators to avoid cell short-circuiting by metallic dendrites at high cycling rates, and 120 μl of the respective lithium or sodium electrolyte specified above. Cell testing was done using a battery cycler (Series 4000, Maccor, USA). Constant-current lithiation/sodiation rates of 0.1, 0.2, 0.5, 1, 2, 3, 4, 5, and 10 C were used, with a lower cutoff voltage of +10 mV vs the lithium/sodium RE potential; the constant-current delithiation/desodiation to an upper cutoff voltage of +1.5 V vs the lithium/sodium RE potential was conducted at a rate that equaled the lithiation/sodiation rate for the two lowest rates (0.1 and 0.2 C) and was then kept constant at 0.2 C for higher lithiation/sodiation rates in order to assure complete delithiation/desodiation of the electrode at the end of each cycle. Three cycles were conducted for each lithiation/sodiation rate, and for the evaluation of the lithiation/sodiation rate performance of the HC electrodes, the third cycle at every C-rate was used. Contrary to the above described impedance experiments, the C-rate is referenced to the same nominal capacity of 280 mAh/g_{HC} for both the Li/HC and the Na/HC half-cells, so that a C-rate of 1 C corresponds to the same current density (0.88 mA cm^{-2}). This was done to allow for a fair comparison of the fast-charging capability (lithiation vs sodiation), as this is known to strongly depend on the geometric current density, as long as the electrode thickness and porosity are kept constant.[41] All experiments were performed in temperature-controlled chambers (Binder, Germany) at 25 °C.

Impedance spectra analysis.—In order to fit the Nyquist impedance spectra of the HC electrodes, an equivalent circuit model was used, which is depicted in Fig. 3c. It consists of a high-frequency resistance element (R$_{HFR}$) as well as of a mono-rail

transmission line that includes a pore resistance (R_{pore}), representing the ionic conduction resistance of the electrolyte within the pores of the HC electrodes, and a charge transfer resistance R_{CT} in parallel to a constant phase element Q_{CT}, similar to the circuit used by Landesfeind et al.[42] The transmission line is simplified by neglecting the electronic resistance rail through the electrode due to the high electronic conductivity of the carbon electrode; for this reason, it will be referred to furtheron as mono-rail transmission line model (mTLM). Fitting of the impedance spectra was performed with a MATLAB-based application ("EIS Breaker" written by J. Landesfeind),[42] which applies an fminsearch MATLAB function using a Nelder-Mead simplex algorithm and modulus weighing.

The pore resistance was determined by fitting the impedance spectrum obtained at the initial OCV prior to the first lithiation/sodiation of the HC electrodes (i.e., at 0% SOC) in Li/HC and Na/HC half-cells. At this condition, the charge transfer resistance of the HC electrode is orders of magnitude larger than R_{pore}, so that the impedance response closely resembles that obtained under so-called blocking conditions. Here, only points measured within a frequency range between ≈30 kHz and ≈25 Hz were taken into account in order to improve the goodness of the fit. The R_{pore} value obtained under these conditions was then fixed during the fitting of R_{CT}, Q_{CT}, and R_{HFR} for the impedance spectra measured over the course of the first (de)lithiation/(de)sodiation cycle. For these fits, frequencies between ≈30 kHz and ≈1 Hz were considered in order to exclude Warburg-like impedance responses at low frequencies and artefacts stemming from the wire-shaped RE geometry at frequencies >30 kHz.[43] The evolution of the hard carbon electrode impedance over extended cycling at C/10 was followed in terms of the high-frequency resistance (R_{HFR}) corrected low-frequency resistance (R_{LFR}), corresponding to the approximate impedance contribution a hard carbon electrode would have in a battery cell (i.e., $R_{anode} = R_{LFR} - R_{HFR}$). This was done by subtracting the real part of the high-frequency resistance (R_{HFR}) taken at 30 kHz from the low-frequency resistance (R_{LFR}), which was defined as the real part of the impedance at the impedance minimum in the low-frequency region of each spectrum, i.e., the transition from the large semi-circle into the Warburg-like linear impedance increase (s. double arrows in Figs. 8a and 8b).

Results and Discussion

First-cycle (de)sodiation and (de)lithiation of a hard carbon electrode.—As already discussed in the literature, the cell impedance of half-cells with a carbon working electrode (WE) and a lithium or sodium counter electrode (CE) is often used to deduce the carbon electrode impedance behavior, neglecting the contribution of the CE,[37,44] even though the impedance of metal electrodes can be quite significant and furthermore changes substantially over the course of cycling.[39] Therefore, in order to study the hard carbon (HC) working electrode impedance *in situ* during the first formation cycle, Na/HC half-cells with 1 M NaPF$_6$ in EC/DMC (1/1 by volume) and Li/HC half-cells with 1 M LiPF$_6$ in EC/EMC (3/7 by weight) were built with micro-reference electrodes to deconvolute the WE and the CE impedance. For the Na/HC half-cells, a tin-wire (μ-TWRE) was used, while a gold-wire reference electrode (μ-GWRE) was used for the Li/HC half-cells. A carbon paper was placed between the lithium or the sodium metal CE and the adjacent separator in order to reduce the impedance of the CE which was shown to be necessary to allow for artefact-free impedance measurements.[39]

Figure 2a shows the cell voltage profiles for the first sodiation and desodiation of a HC electrode in a Na/HC half-cell as a function of the specific capacity of the HC active material obtained for a constant-current (de)sodiation rate of 0.1 C (referenced to a nominal HC (de)sodiation capacity of 280 mAh/g$_{HC}$) and with a lower cell cutoff potential of 10 mV$_{cell}$. The voltage was controlled vs the metal CE and the cycling of the cell was interrupted at cell voltages
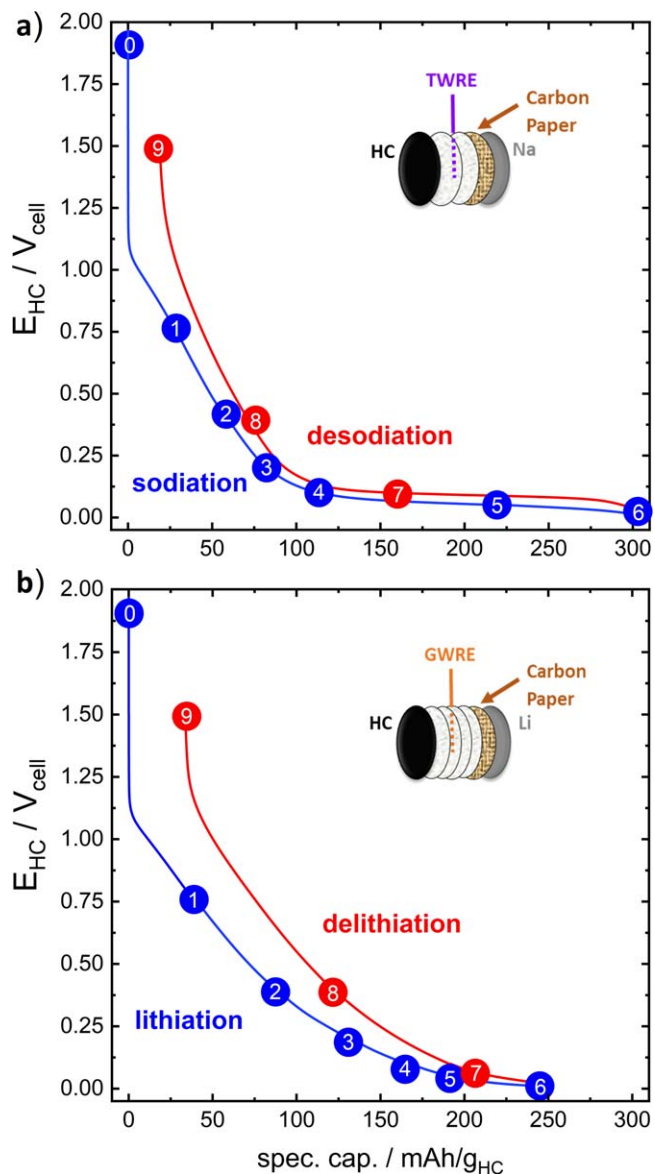

Figure 2. (a) Cell voltage (E$_{cell}$) of a Na/HC half-cell vs capacity during the first-cycle (de)sodiation at a rate of 0.1 C in EC/DMC (1/1 by volume) with 1 M NaPF$_6$ and with a lower cell voltage cutoff potential of 10 mV$_{cell}$. The experiment is conducted in a Swagelok®-type T-cell equipped with a μ-TWRE that is placed in between two glass fiber separators and a carbon paper that is placed between the sodium metal CE and the adjacent separator (see scheme in the inset). At the cell potentials labelled from 1–9 in the graph, the cycling procedure was stopped and potential-controlled electrochemical impedance (PEIS) spectra were acquired after an OCV period of 30 min; the point labeled 0 marks the initial OCV prior to the first sodiation. (b) Analogous measurements for a Li/HC half-cell with 1 M LiPF$_6$ in EC/EMC (3/7 by weight), using a μ-GWRE placed between two glass fiber separators (s. inset).

of 750, 400, 200, 100, 50, and 10 mV$_{cell}$ during sodiation and at 100, 400, and 1500 mV$_{cell}$ during desodiation. At each of these voltage setpoints, the cell was rested for 30 min at OCV, followed by an *in situ* potential-controlled electrochemical impedance (PEIS) measurement, whereby the voltage perturbation amplitude was controlled vs the μ-TWRE. For the Na/HC half cell (Fig. 2a), the cell voltage curves during sodiation (blue line/symbols) and during desodiation (red line/symbols) exhibit a sloping profile that transitions into a nearly flat low-voltage region at cell voltages below ≈100 mV and that extends over roughly two thirds of the total (de)

sodiation capacity. These types of voltage profiles are commonly observed for the (de)sodiation of HC electrodes. The first-cycle coulombic efficiency (CE) for the Na/HC half-cell is ≈92%.

The analogous experiment at 0.1 C was conducted for a Li/HC half-cell equipped with a μ-GWRE (Fig. 2b), whereby the C-rate in the case of lithium is referenced to the nominal HC (de)lithiation capacity of 220 mAh/g$_{HC}$. Currently, we do not know the reason why the (de)sodiation capacities are relatively high compared to the (de)lithiation capacities. However, since this is a commercial product (Kuraray, Japan), it might be that the carbon material was developed with a focus on its application in SIBs.

In contrast to the Na/HC half-cell, the cell voltage curve during lithiation (blue line/symbols) and delithiation (red line/symbols) does not show an extended low-voltage plateau, as it was observed for the Na/HC half-cell between ≈100–300 mAh/g$_{HC}$, and the sloping voltage region extends almost all the way to the lower cutoff potential of 10 mV$_{cell}$. The reason for this difference is currently not known and might be a specific property of this type of hard carbon. The first-cycle lithiation capacity of ≈260 mAh/g$_{HC}$ is lower than that observed for the Na/HC half-cell (≈300 mAh/g$_{HC}$), as is the first-cycle coulombic efficiency of ≈84% (≈92% for the Na/HC half-cell).

Determining the pore resistance R_{pore} of hard carbon electrodes in Na/HC and Li/HC half-cells.—The ionic resistance in the electrolyte phase within the pores of the hard carbon electrodes (R_{pore}) used in the Na/HC and Li/HC half-cells was determined at OCV prior to any sodiation/lithiation of the HC electrodes, i.e., at the initial 0% SOC condition, corresponding to the points labeled with 0 in Figs. 2a and 2b. As the charge transfer resistance (R_{CT}) in this case should be very large, these conditions should closely approach the so-called blocking conditions, which allow for the most precise evaluation of R_{pore} from a fit of the hard carbon electrode impedance data (recorded by PEIS at OCV) to the equivalent circuit depicted in Fig. 3c, as was demonstrated by Landesfeind et al.[42] and Linsenmann et al.[37] The equivalent circuit consists of a mono-rail transmission line model (mTLM) composed of an ionic conduction

rail represented by R_{pore}, of parallel circuit elements of a charge transfer resistance (R_{CT}) and a constant phase element (Q_{CT}) that represents the double-layer capacitance, and of an electronic conduction rail with a negligible electronic resistance corresponding to the highly conductive hard carbon particles. A single resistance element is added to the electronic rail of the mTLM to represent the high frequency resistance (R_{HFR}) that describes the sum of the external electronic contact resistance of the HC anode electrode and of the effective ionic resistance in the separator between the μ-RE and the HC electrode.

The measured impedance data of the hard carbon electrode (symbols) and the corresponding equivalent circuit fit (dashed lines) for a Na/HC and a Li/HC cell are depicted in Figs. 3a and 3b, respectively. In order to obtain a stable fit, rather than setting the electronic resistance of the electronic rail (s. Fig. 3c) to zero, it was set to a very small value of 0.001 Ωcm^2, which, as will be shown, is negligible compared to the measured R_{pore} values. For the hard carbon electrodes prepared in this study (s. Experimental section), we obtain a HC electrode pore resistance of 4.8 ± 0.5 Ωcm^2 in the Na/HC half-cells and of 4.6 ± 0.6 Ωcm^2 in the Li/HC half-cells (each based on two repeat experiments, whereby the error was obtained by including both the error of the cell-to-cell variability and the fitting error (s. Table I)), which are essentially identical within the error of measurement (the values obtained for the impedance data fit shown in Figs. 3a and 3b are given in Table I). As the HC electrodes for all the cells are nominally identical with regards to thickness and porosity, equal R_{pore} values of the HC electrode measured in Na/HC and in Li/HC half-cells would suggest equal conductivities of the two electrolytes. The latter is indeed the case, with an electrolyte conductivity of 8.2 mS cm^{-1} for the sodium electrolyte and of 8.3 mS cm^{-1} for the lithium electrolyte at 25 °C. The other fitting parameters are summarized in Table I for one data set each for both cell types (that shown in Figs. 3a and 3b), showing that the charge transfer resistance (R_{CT}) is indeed orders of magnitude larger than R_{pore}, so that blocking conditions are closely met; furthermore, the values of the constant phase element exponents α_{CT} are still reasonably close to 1, as is observed for most LIB electrodes.[42,45]
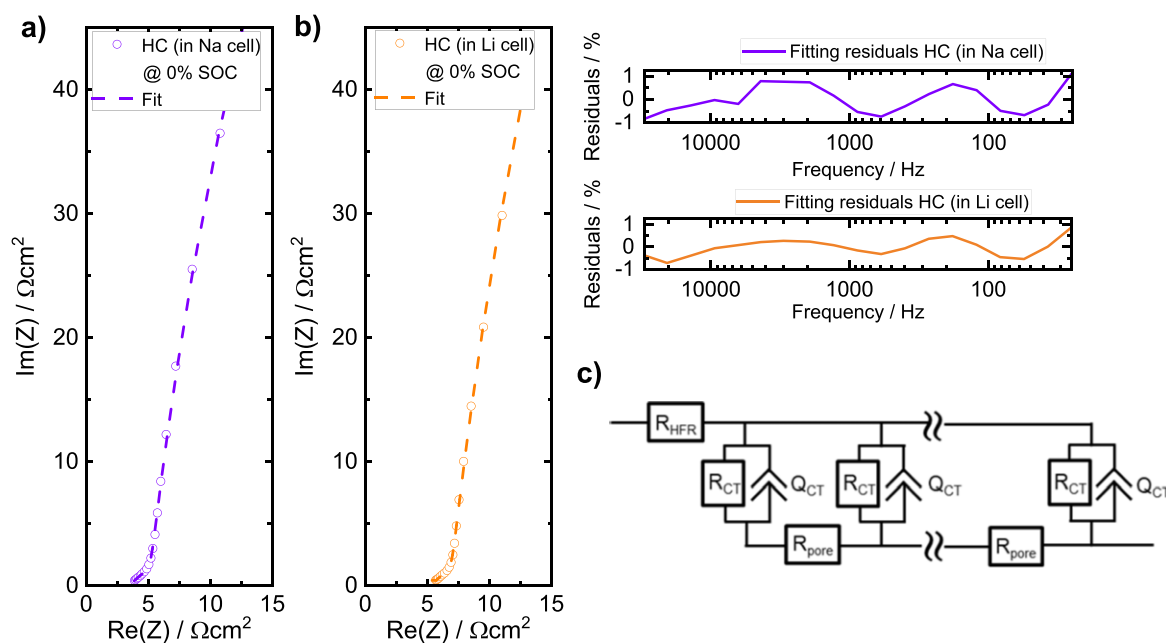

Figure 3. (a) Nyquist plot (purple symbols) of the hard carbon electrode impedance in a Na/HC half-cell with a μ-TWRE (s. inset of Fig. 2a at 0% SOC prior to the first sodiation (≡point 0 in Fig. 2a); (b) Nyquist plot (orange symbols) of the hard carbon electrode impedance in a Li/HC half-cell with a μ-GWRE (s. inset of Fig. 2b) at 0% SOC prior to the first lithiation (≡point 0 in Fig. 2b). The plotted PEIS data (symbols) were acquired at OCV and range from ≈30 kHz to ≈25 Hz. The fit to the equivalent circuit depicted in panel (c) (dashed lines) was performed in the same frequency range, whereby the residuals of the fit vs frequency are given in the panels next to the Nyquist plots. (c) The equivalent circuit used for fitting consists of a high-frequency resistance element (R_{HFR}), a mono-rail transmission line model (mTLM) with R/Q-elements (in parallel) that are composed of a charge transfer resistance (R_{CT}) and a constant phase element (Q_{CT}), and pore resistance elements (R_{pore}) that represent the ionic conduction resistance in the electrolyte phase in the pores of the electrode.

Table I. Fitting parameters and their obtained values for the hard carbon impedance spectra at 0% SOC prior to sodiation (from Fig. 3a) or lithiation (from Fig. 3b), using the equivalent circuit depicted in Fig. 3c. Here, R_{HFR} is the high-frequency resistance, R_{CT} is the charge transfer resistance of the hard carbon electrode, Q_{CT} is the constant phase element magnitude, and α_{CT} is the constant phase exponent. The errors (in %) are the fitting errors obtained by the least-squares minimization fitting method. Note that four glass fiber separators were used in the case of the Li/HC half-cell, compared to only two that were used in the Na/HC cell, explaining the nearly 2-fold higher R_{HFR} value.

Parameter	Na/HC Half-cell		Li/HC Half-cell	
	Value	Error/%	Value	Error/%
$R_{HFR}/\Omega cm^2$	3.5	4.2	5.3	9.5
$R_{pore}/\Omega cm^2$	4.5	10	4.6	13
$R_{CT}/k\Omega cm^2$	1.0	24	1.8	13
$Q_{CT}/mF \cdot s^{(\alpha_{CT}-1)}/cm^2$	0.18	5.2	0.22	2.6
$\alpha_{CT}/$	0.92	1.0	0.92	0.6

The nearly 2-fold higher R_{HFR} value obtained for the Li/HC cell is due to the fact that four glass fiber separators were used in this case, compared to only two that were used in the Na/HC cell. Considering the almost identical conductivities of the sodium and of the lithium ion electrolyte (s. above), one would expect a close to 2-fold higher R_{HFR} for the Li/HC compared to the Na/HC half-cells. However, also earlier studies[37,40] have shown that the compression of multiple glass fiber separators can vary significantly from cell to cell due to minor differences in cell stack compression.

Note that the errors given in Table I represent the fitting error determined by the MATLAB-based fitting script (using an fmin-search MATLAB function, applying a Nelder-Mead simplex algorithm and modulus weighing), and therefore represents the error induced by fitting and not a cell-to-cell variation; both errors are included in the above given average R_{pore} values of the HC electrodes in the Na/HC and the Li/HC half-cells.

SOC-dependent evolution of the hard carbon electrode impedance in Na/HC and HC/Li half-cells.—The Nyquist spectra of the HC electrode impedances recorded at the OCV points labelled 0–9 (s. Figs. 2a and 2b) are displayed in Figs. 4 and 5. Figure 4 shows the spectra for sodiation (a) and desodiation (b) recorded for the Na/HC half-cell, and Fig. 5 for lithiation (a) and delithiation (b) in the Li/HC half-cell. For both half-cells, the HC electrode impedance decreases with increasing SOC during the first sodiation/lithiation half-cycle and then increases again during the subsequent desodiation/delithiation half-cycle. For all the Nyquist plots of the hard carbon electrodes, three distinct features can be distinguished: i) an x-axis intercept of the high-frequency part of the spectra, marking the high frequency resistance (R_{HFR}); ii) a short ≈45°-line at high frequencies that originates from the pore resistance (R_{pore})[42] already described above (s. Fig. 3); and, iii) a semi-circle at mid and low frequencies that is caused by the charge transfer process and whose diameter decreases with decreasing charge transfer resistance. As already discussed in the context of Table I, the higher R_{HFR} value in the Li/HC half-cell is due to the fact that four glass fiber separators were used in Li/HC half-cells compared to only two glass fiber separators in the Na/HC half-cells.

The data in Figs. 4 and 5 suggest that the HC electrode impedance decreases continuously with decreasing cell potential, i.e., with decreasing HC potential or with increasing hard carbon SOC (a quantitative analysis will be presented in the next section). Unfortunately, to the best of our knowledge, no data on the impedance of hard carbon anodes upon (de)sodiation exist in the literature (there are some full-cell impedance measurements,[46] but these do not allow for a deconvolution of the anode impedance).
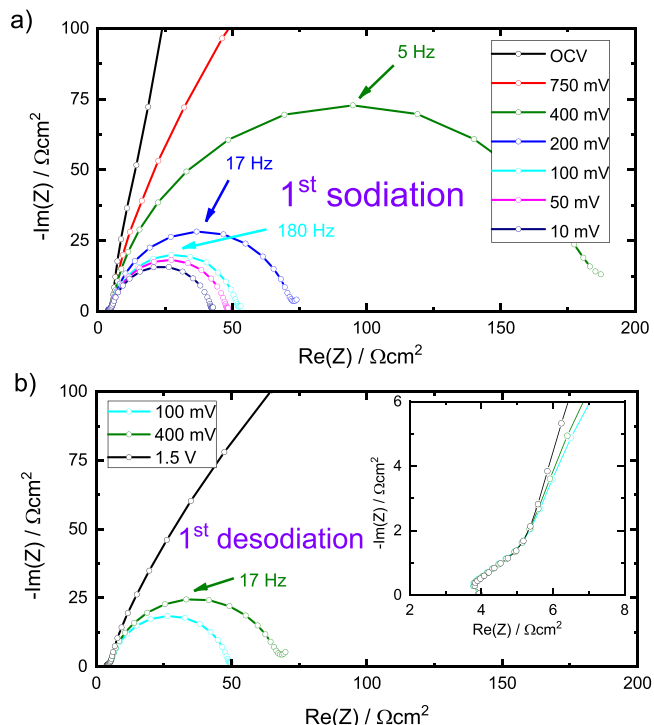
Figure 4. Nyquist plots of the HC impedance in Na/HC half-cells recorded during the first-cycle (de)sodiation at the OCV points labeled with 0–9 that are shown in Fig. 2a, using a frequency range between 30 kHz and 0.1 Hz: (a) sodiation, (b) desodiation. The inset in (b) shows the magnification of the high-frequency region, depicting the short ≈45°-line part of the spectra. The experiments were conducted at 25 °C with an EC/DEC (1/1 by volume) + 1 M NaPF$_6$ electrolyte.
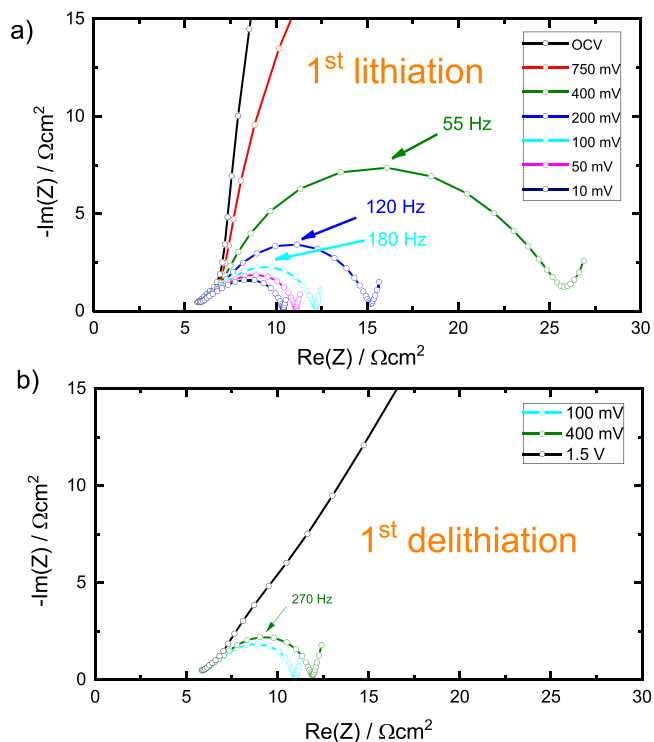
Figure 5. Nyquist plots of the HC impedance in Li/HC half-cells recorded during the first-cycle (de)lithiation at the OCV points labeled with 0–9 that are shown in Fig. 2b, using a frequency range between 30 kHz and 0.1 Hz: (a) lithiation, (b) delithiation. The experiments were conducted at 25 °C with an EC/EMC (3/7 by mass) + 1 M LiPF$_6$ electrolyte.

Even in the case of carbon based anodes in lithium-ion batteries, very few studies exist where the impedance of carbon based anodes is measured *in situ* as a function of SOC during the first lithiation. For example, Dollé et al.[47] used an LFP-based RE for *in situ* measurements of the impedance of an MCMB-type graphite anode, reporting that the graphite electrode impedance is increasing with SOC between 0.55 and 0.02 V vs Li^+/Li. On the contrary, Song et al.[44] show that the impedance of their graphite electrode measured with a Li μ-RE first decreases with increasing SOC, reaching a minimum at 0.094 V vs Li^+/Li, and then increases again. They, however, employ a mixture of ethylene carbonate (EC) and γ-butyrolactone as electrolyte in contrast to Dollé et al.,[47] who use EC and ethylmethyl carbonate (EMC). To the best of our knowledge, the only *in situ* impedance study of a HC anode as a function of SOC during the electrode formation vs lithium was published by Barsoukov et al.[48] Here, the authors analyzed impedance spectra of an MCMB, a graphite, and a hard carbon electrode recorded during the first lithiation by means of a Li μ-RE placed within a custom-made LIB cell. They find that for both graphite and hard carbon the electrode impedance first decreases upon lithiation and then continuously grows with increasing SOC. However, the reliability of the cell setup is questionable, since the MCMB shows an irreversible capacity of 47% in the first cycle and only a specific capacity of 221 mAh g^{-1}, whereas coulombic inefficiencies of <10% and capacities of $\approx$330 mAh g^{-1} [49] are generally reported for MCMB active materials in the literature.[50,51] In so far unpublished EIS experiments on (de)lithiation of artificial graphite electrodes performed in our group, we also find the trend that the electrode impedance decreases with increasing SOC during the first cycle (measured in half-cells using a μ-GWRE). In the following section, we will fit the hard carbon impedance spectra shown in Figs. 4 and 5 to the equivalent circuit model shown in Fig. 3c in order to extract the charge transfer resistance and to determine its first-cycle variation with SOC.

Charge transfer resistance (R_{CT}) of HC electrodes vs SOC in Na/HC and Li/HC half-cells.—By comparing the Nyquist impedance spectra in Figs. 4 and 5, it becomes clear that the magnitude of the hard carbon electrode impedance is significantly larger for the Na/HC compared to the Li/HC half-cell. In order to precisely evaluate the value of the charge transfer resistance (R_{CT}) and to compare the obtained values for (de)sodiation and (de)lithiation, the impedance spectra in Figs. 4 and 5 were fitted using the equivalent circuit shown in Fig. 3c. In this case, the pore resistance R_{pore} was fixed to the value obtained from the spectra in blocking conditions (for one set of experiments, these are shown in Table I, while their average values are 4.8 ± 0.5 Ωcm^2 and 4.6 ± 0.6 Ωcm^2 for the Na/HC and the Li/HC half–cell). Exemplary fits for the spectra recorded after the first sodiation/lithiation of a Na/HC and a Li/HC half-cell to a cell potential of 10 mV are depicted in Fig. 6a (purple symbols (data) and dashed line (fit)) and 6b (orange symbols (data) and dashed line (fit)), respectively. Especially in the case of the HC impedance in the Li/HC half-cell (s. Fig. 3b), it becomes clear that the true value of R_{CT} can only be determined by a fit of the impedance data to a transmission line model since the $\approx$45°-part at high frequencies, that reflects the contribution from R_{pore}, is partially overlapping with the semi-circle that originates from the charge transfer resistance.

The thus determined R_{CT} values of the HC electrode during the first cycle in both the Na/HC (purple symbols/lines in Fig. 6c) and the Li/HC (orange symbols/lines) half-cell rapidly decrease upon the initial sodiation/lithiation to $\approx$100 mAh/g_{HC}, after which they gradually decrease until the lower cutoff potential of 10 mV_{cell} is reached. During the subsequent desodiation/delithiation, the R_{CT} values closely follow those during sodiation/lithiation. The absolute R_{CT} values of the hard carbon electrodes at 100% SOC are $\approx$10-fold higher for (de)sodiation compared to (de)lithiation. For example, at 100% SOC (i.e., at a cell potential of 10 mV), R_{CT} is 37.4 ± 0.1 Ωcm^2 for the Na/HC half-cell compared to only 3.5 ± 0.03 Ωcm^2

for the Li/HC half-cell. As one would expect, the high-frequency resistance R_{HFR} (lower panel of Fig. 7c) remains constant throughout this cycle. In Table II, the fitting parameters for the fits shown in Figs. 6a and 6b are tabulated together with the fitting errors.

HC electrode impedance evolution over the course of cycling of Na/HC and Li/HC half-cells.—Figure 7a shows the specific desodiation/delithiation capacities and the coulombic efficiencies of Na/HC (purple symbols) and Li/HC half-cells (orange symbols) over extended cycling at a rate of 0.1 C between 1.5 and 0.01 V_{cell}. The slow cycling rate was chosen due to the additional resistance added to the electrode stack by the carbon paper free-standing electrode attached to the metallic CE (s. Fig. 1a), which was necessary to allow for *in situ* EIS measurements with μ-REs (i.e., the μ-TWRE and the μ-GWRE), as was discussed in the Experimental section.[39] Cycling the cells at higher C-rates would lead to increased ohmic potential drops that negatively affect the cycling capacity of the cell and would thus artificially reduce the HC electrode capacity from its intrinsic value in the absence of this added resistive element (i.e., the carbon fiber paper) in the cell. For both the Na/HC and the Li/HC half-cells, the HC electrode shows a fairly stable cycling behavior over 52 cycles. In case of the Li/HC half-cells, the formation of an effective SEI seems to be somewhat slower, since the coulombic efficiency over the first $\approx$4 cycles is significantly lower that that observed for Na/HC half-cells. For both cell types, the cycling stability is very similar, with desodiation/delithiation capacity losses of $\approx$18 mAh/g_{HC} between cycle 1 and 52, corresponding to a relative capacity loss of $\approx$6% for the Na/HC half-cells and of $\approx$8% for the Li/HC half-cells.

Figures 8a and 8b show the evolution of HC impedance spectra over extended cycling (cycle 1, 2, 12, and 52), measured in Na/HC and Li/HC half-cells at OCV after sodiation/lithiation to a cell voltage of 100 mV_{cell}, followed by a relaxation phase of 30 min (for the first cycle, this would correspond to point 4 in Figs. 2a and 2b). In the case of the Li/HC half-cell (Fig. 8b), the shape of the hard carbon impedance spectra, consisting of a pore resistance R_{pore} indicated by a $\approx$45°-line which transitions into a large semi-circle originating from a charge transfer resistance R_{CT}, does not vary over cycling; however, the diameter of the semi-circle, and therefore the magnitude of R_{CT} is changing. In contrast, in the case of the Na/HC half-cell, the large semi-circle starts to split into a smaller one at higher frequencies and a larger one at lower frequencies after $\approx$30 cycles (shown for cycle 52 in Fig. 8a). Unfortunately, we currently do not know the origin of this additional impedance feature; as it is reproducible and evolves only upon extended (de)sodiation, we believe that it reflects a hitherto unknown ageing mechanism of HC anodes upon extended sodiation/desodiation cycles. Because of the appearance of this second semi-circle, the HC spectra in the Na/HC half-cell cannot be fitted by the equivalent circuit depicted in Fig. 3c, which is the reason why the evolution of R_{CT} could not be evaluated over long-term cycling. Instead, we evaluated the approximate impedance contribution of a HC anode in a battery cell, defined as $R_{anode} = R_{LFR} - R_{HFR}$ (s. purple/orange double arrow in Figs. 8a/8b), whereby R_{HFR} is approximated by the real part of the impedance at 30 kHz and R_{LFR} is approximated by the real part of the impedance at the transition from the large low-frequency semi-circle to the Warburg-like linear impedance increase. Thereby, the impedance of the separator (closely corresponding to the impedance at 30 kHz) and contributions from the Warburg-like impedance response at rather low frequencies are excluded, so that the remaining impedance should be a reasonable approximation of the impedance contribution of a hard carbon anode in a battery cell. The thus determined R_{anode} values of the HC electrode are plotted as a function of cycle number in Fig. 8c for the Na/HC half-cells (purple symbols) and the Li/HC half-cells (orange symbols). For both the Na/HC and the Li/HC half-cells, R_{anode} decreases by $\approx$25% after the first cycle, which could be explained by an increase of the specific surface area of the HC active material during the first cycles via opening of initially inaccessible pores in the material, which in
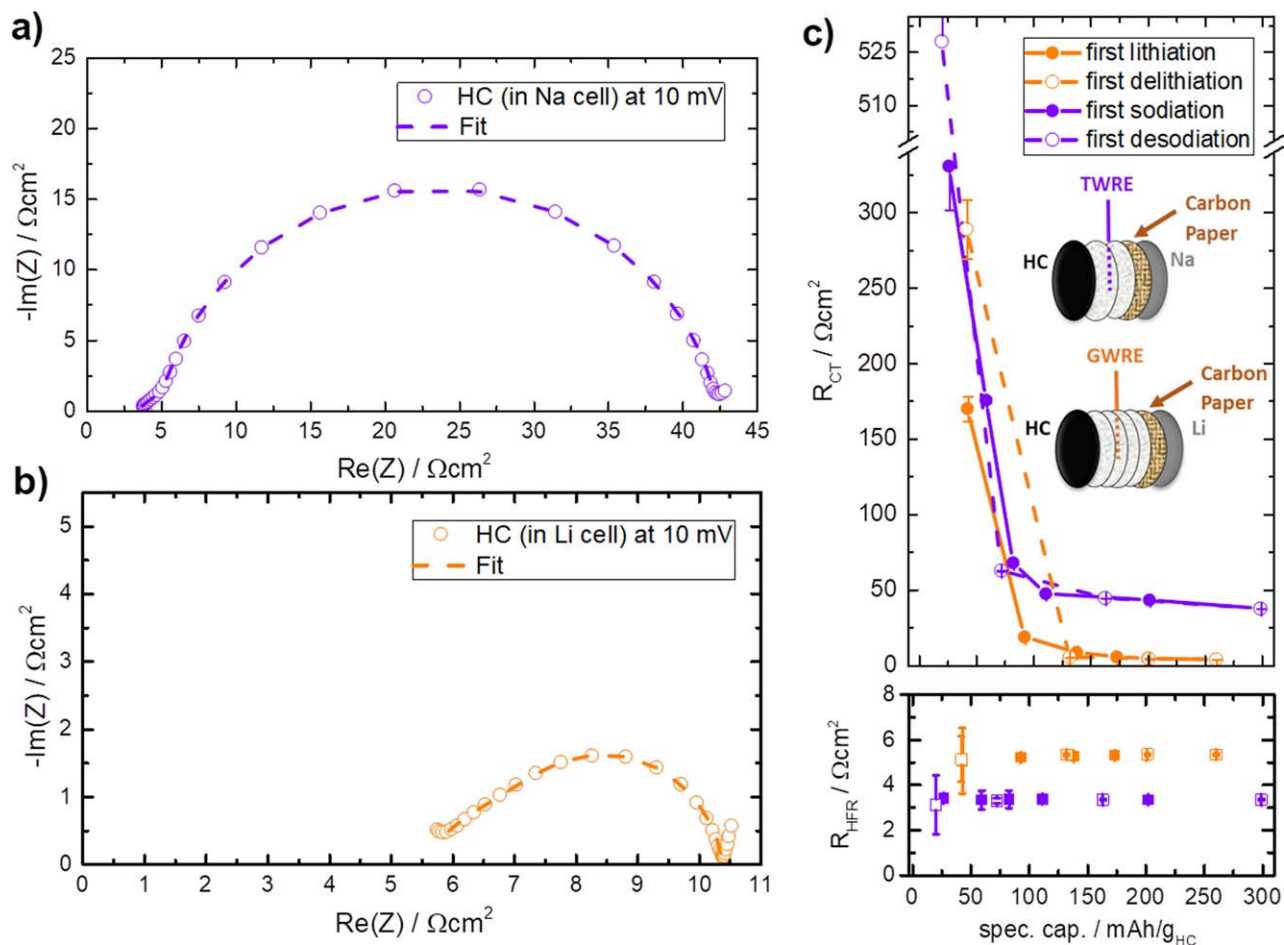
Figure 6. Analysis of the hard carbon electrode impedance data for the first-cycle sodiation/lithiation at 0.1 C and 25 °C (the corresponding voltage profiles and impedance spectra are shown in Fig. 2 as well as in Figs. 4 and 5). The left panels show a fit (dashed lines) of the HC electrode impedance data (symbols) acquired at 10 mV$_{cell}$ after a 30 min OCV phase (≡ points 6 in Fig. 2), using the equivalent circuit model depicted in Fig. 3c: (a) for the Na/HC half-cell using the μ-TWRE; (b) for the Li/HC half-cell using the μ-GWRE. The thus obtained fitting parameters are given in Table II. (c) Area normalized charge transfer resistance (R$_{CT}$) and high-frequency resistance (R$_{HFR}$) vs SOC in the first cycle, determined by fitting the HC impedance spectra recorded for the Na/HC half-cell (purple symbols/lines; spectra shown in Fig. 4) and for the Li/HC half-cell (orange symbols/lines; spectra shown in Fig. 5) to the equivalent circuit model shown in Fig. 3c; the R$_{pore}$ values were set to those determined in blocking conditions (s. Table I). The error bars represent the fitting errors obtained by the least square fitting method.
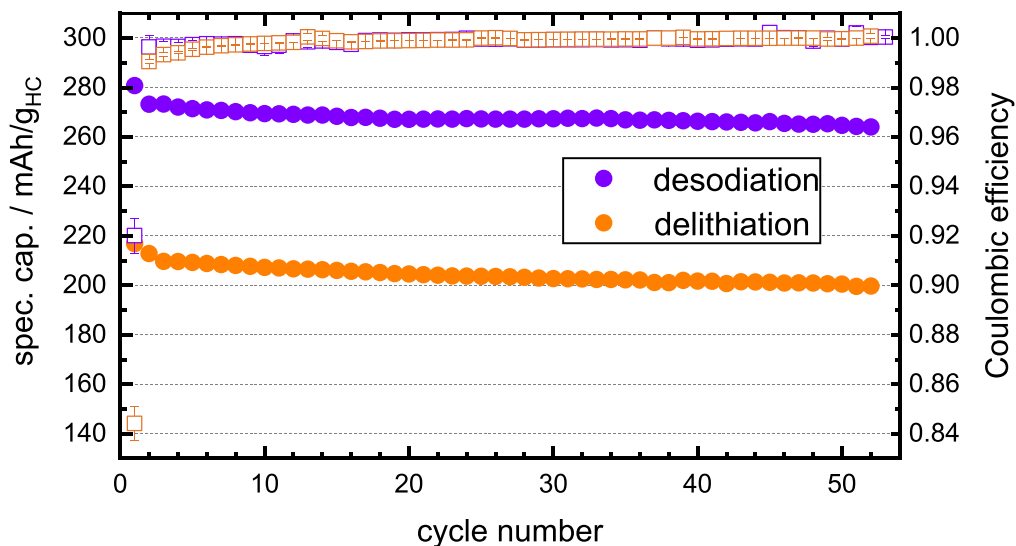

Figure 7. Specific desodiation (purple symbols) and delithiation (orange symbols) capacities as well as coulombic efficiencies vs cycle number of Na/HC and Li/HC half-cells, respectively, cycled at 0.1 C between 1.5 and 0.01 V$_{cell}$.

Table II. Fitting parameters and their obtained values for the hard carbon impedance spectra shown in Figs. 6a and 6b, measured after the first sodiation of Na/HC and the first lithiation of Li/HC half-cells to a cell potential of 10 mV$_{cell}$ ($\equiv$ 100% SOC), using the equivalent circuit depicted in Fig. 3c. Here, R$_{HFR}$ is the high-frequency resistance, R$_{CT}$ is the charge transfer resistance of the hard carbon electrode, Q$_{CT}$ is the constant phase magnitude, and α_{CT} is the constant phase exponent. R$_{pore}$ was fixed to the values obtained in blocking conditions (s. Table I), based on the impedance spectra shown in Figs. 3a and 3b. The error is based on the fitting errors obtained by the least square fitting method.

	HC/Na Half-cell		HC/Li Half-cell	
Parameter	Value	Error/%	Value	Error/%
R$_{pore}$/Ωcm^2 (from Table I)	4.5	10	4.6	13
R$_{HFR}$/Ωcm^2	3.4	1.0	5.4	0.5
R$_{CT}$/Ωcm^2	37.4	0.2	3.5	0.9
Q$_{CT}$/mF·s$^{(\alpha_{CT}-1)}$/cm^2	0.25	1.1	0.3	5.5
α_{CT}/	0.89	0.2	0.89	1.0

turn would facilitate charge transfer into the active material particles.[37] As was already noted in the discussion of the data in Fig. 6c, the HC impedance, dominated by a charge transfer resistance, is significantly higher for the Na/HC compared to the Li/HC half-cells. Over the course of cycling, the hard carbon anode impedance values for both cell types gradually increase, and after 52 cycles the hard carbon impedance R$_{anode}$ is still $\approx$5-fold higher for the Na/HC than for the Li/HC half-cells.

Sodiation/lithiation rate capability of HC electrodes in Na/HC and Li/HC half-cells.—The higher hard carbon charge transfer resistances in Na/HC vs Li/HC half-cells (s. Figs. 6 and 7) are expected to result in higher kinetic overpotentials of the hard carbon electrode in Na/HC half-cells. Since the kinetic overpotential lowers the hard carbon electrode potential during sodiation (or lithiation), the hard carbon electrode potential will decrease below 0 V vs Na$^+$/Na (or Li$^+$/Li) at lower and lower SOC values, as the C-rate and thus the current density is increased. Therefore, the sodiation (or lithiation) capacity at which the hard carbon electrode potential decreases below 0 V vs Na$^+$/Na (or Li$^+$/Li) marks the maximum accessible capacity that can be reached under constant-current charging conditions without risking sodium (or lithium) plating, which is detrimental to cycle-life and safety. The relationship between the thus defined maximum accessible capacity of a hard carbon electrode vs C-rate, however, cannot be determined by simply monitoring the cell voltage, since the overpotentials of a sodium or lithium metal counter electrode can be very high at high current densities.[39] Therefore, the hard carbon electrode cutoff potential during the following rate tests in Na/HC and Li/HC half-cells was controlled to +10 mV vs a metallic sodium or lithium RE, respectively, rather than vs the cell voltage, analogous to the procedure described by Landesfeind et al.[52] Since kinetic as well as transport-related overpotentials in general increase with current density, the C-rates in these experiments were referenced to the same nominal capacity of 280 mAh/g$_{HC}$, allowing for a direct comparison of the rate capability for sodiation and lithiation in Na/HC and Li/HC half-cells, respectively. In this case, a rate of 1 C corresponds to a current density of 0.88 mA cm^{-2}. In order to avoid cell short-circuiting by sodium/lithium dendrites originating from the sodium/lithium metal counter electrode (expected to occur for current densities larger than $\approx$1 mA cm^{-2},[53] i.e., at rates larger than $\approx$1.15 C in our case), the distance between WE and CE was increased to $\approx$800 μm by using four glass fiber separators (compared to the more commonly employed two glass fiber separators).

Figure 9a shows the C-rate dependence of the accessible specific capacity for sodiation (purple symbols/line) and lithiation (orange symbols/lines) of Na/HC and Li/HC half-cells, respectively, using a lower cutoff potential of +10 mV vs Li$^+$/Li and Na$^+$/Na, respectively. For the Na/HC half-cell, the capacity drops rapidly beyond a rate of 1 C, which can be explained by the high charge transfer resistance R$_{CT}$ of the HC electrode for sodiation ($\approx$50 Ωcm^2, s. Fig. 6c). For example, at a current density of 1.76 mA cm^{-2} ($\equiv$2 C),

this equates to a kinetic overpotential of $\approx$90 mV. The consequence of this can be estimated by considering the voltage vs capacity curve shown in Fig. 2a that was recorded at only 0.1 C corresponding to only $\approx$0.09 mA cm^{-2}, in which case the overpotentials of both the Na and the HC electrode can be considered negligible, so that the cell voltage should be close to the HC electrode potential vs the Na$^+$/Na reference potential. Shifting this voltage profile negative by $\approx$90 mV, *viz.*, by the projected kinetic overpotential at 2 C, means that point 4 in Fig. 2a (at $\approx$115 mAh/g$_{HC}$) that marks a cell voltage of 100 mV (corresponding to also $\approx$100 mV vs Na$^+$/Na) would be expected to drop to $\approx$10 mV vs Na$^+$/Na, corresponding to the cutoff potential of our Na/HC half-cell in the rate test shown in Fig. 8a, where a sodiation capacity of $\approx$150 mAh/g$_{HC}$ was obtained at 2 C. Considering this rough estimate, this is reasonably close to the projected $\approx$115 mAh/g$_{HC}$ based on the data at 0.1 C, suggesting that the high R$_{CT}$ of the hard carbon electrode in the Na/HC half-cell is the origin for the rapid drop in capacity between 1 and 2 C. This suggests that based on kinetic overpotential constraints, the sodiation rate capability of the here used hard carbon material would be limited to somewhere between $\approx$1–2 C, even in the absence of mass-transport limitations (these would become more important for higher, more application-relevant HC areal capacities, resulting in thicker electrodes and higher current densities for a given C-rate[41]).

On the other hand, for the Li/HC half-cell, the lithiation capacity decreases more gradually and does not show such a rapid capacity drop, consistent with its $\approx$10-fold lower charge transfer resistance (s. Fig. 6c). This becomes more apparent when normalizing the capacity to the capacity at 0.1 C, as shown in Fig. 9b.

Conclusions

In the present work, we utilized *in situ* electrochemical impedance spectroscopy (EIS) to investigate the impedance change of a commercial hard carbon (HC) active material in Na/HC and Li/HC half-cells. For the Na/HC half-cells, a sodiated tin-wire reference electrode (μ-TWRE) was employed, whereas in the case of the Li/HC half-cells, a lithiated gold wire reference electrode (μ-GWRE) was used to acquire electrode-resolved impedance data. Both in the case of Na/HC and Li/HC, we determined the pore resistance (R$_{pore}$) of the anode prior to the first sodiation/lithiation, where so-called blocking electrode conditions are observed. Subsequently, we monitored the charge transfer resistance R$_{CT}$ as a function of the state-of-charge (SOC) and potential during the first cycle (de) sodiation and (de)lithiation by fitting the impedance spectra with a simple equivalent circuit consisting of a mono-rail transmission line model (mTML) and a high-frequency resistance (R$_{HFR}$). R$_{CT}$ clearly dominates the total electrode impedance for both (de)sodiated and (de)lithiated HC and it reversibly decreases/increases with in-creasing/decreasing SOC during the first cycle. At the end of the first sodiation/lithiation half-cycle, i.e., at 100% SOC, R$_{CT}$ was found to be a factor of $\approx$10 larger for sodiation compared to lithiation of the same hard carbon active material. Note that other types of electrolytes, especially when using additives, might affect
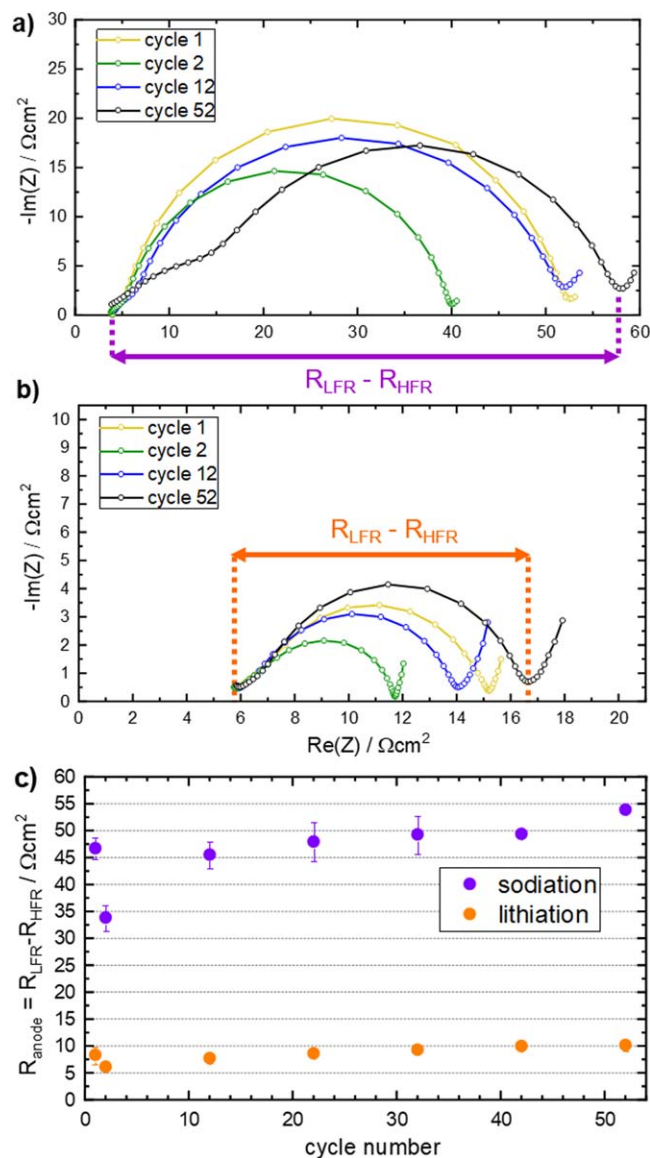
Figure 8. (a) Nyquist plots of the HC impedance in a Na/HC half-cell recorded during sodiation (measured at OCV after cycling to a cell voltage of 100 mV$_{cell}$) for cycle 1 (yellow), 2 (green), 12 (blue), and 52 (black) within a frequency range between 30 kHz and 0.1 Hz, (b) Nyquist plots of the HC impedance in a Li/HC half-cell using the same cycling and EIS measurement procedure, (c) hard carbon electrode impedance R$_{anode}$ evolution during cycling at a rate of 0.1 C between 1.5 and 0.01 V$_{cell}$ (s. Fig. 7) for sodiation (purple) and lithiation (orange). Here, we defined the approximate impedance contribution of a HC anode in a battery cell as R$_{anode}$ = R$_{LFR}$ − R$_{HFR}$ (s. purple/orange double arrows in Figs. 8a/8b), where R$_{LFR}$ is taken as the real part of the impedance at the impedance minimum in the low-frequency region, i.e., the transition from the large semi-circle to the Warburg-like linear impedance increase, and R$_{HFR}$ is taken as the real part of the impedance value measured at 30 kHz. The error bars represent the deviation from the average impedance of two nominally identical cells.

the observed electrode resistances. However, the electrolytes used in this study, i.e., EC/DMC + 1 M NaPF$_6$ and EC/EMC + 1 M LiPF$_6$, were chosen to be very similar in order to assure reasonable comparability between the Na/HC and Li/HC cells.

Furthermore, we traced the impedance evolution of the HC electrode (R$_{anode}$ = R$_{LFR}$ − R$_{HFR}$), defined as the difference of a low-frequency resistance R$_{LFR}$ (real part of the impedance in the low-frequency region where the transition from the large semi-circle into the Warburg-like linear impedance occurs) and a high-frequency resistance R$_{HFR}$ (real part of the impedance at 30 kHz), over
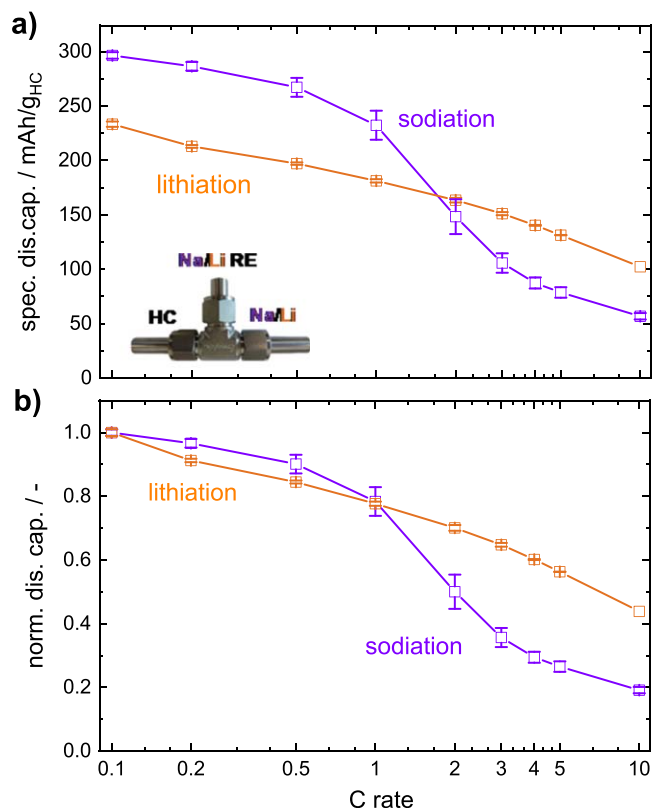

Figure 9. (a) Peukert plot for the sodiation (purple) and lithiation (orange) capacity vs C-rate of hard carbon electrodes in Na/HC and Li/HC half-cells, whereby the capacity values are determined once the HC electrode potential reaches 10 mV vs a sodium and a lithium reference electrode, respectively. The sodiation/lithiation rates were 0.1, 0.2, 0.5, 1, 2, 3, 4, 5 and 10 C for three cylces each, plotting the capacity for the third cycle. The desodiation/delithiation rate was fixed to 0.2 C, except for the sodiation/lithiation rate of 0.1 C, where it was fixed to 0.1 C. For both sodiation and lithiation the C-rate is referenced to 280 mAh/g$_{HC}$, such that a C-rate of 1 C corresponds to the same current density for sodiation and lithiation (0.88 mA cm^{-2}). (b) Data from (a) normalized by the specific sodiation/lithiation capacity obtained at 0.1 C.

52 cycles via EIS measurements at a constant cell potential of ≈100 mV$_{cell}$. For both the Li/HC and the Na/HC half-cells, R$_{anode}$ first decreases after the first cycle and then gradually increases during long-term cycling (52 cycles) and at this potential (corresponding to mid-SOC values) is on average a factor of ≈5 higher for the Na/HC cells compared to the Li/HC cell.

The larger R$_{anode}$ values of the latter are reflected in the lower rate performance of the HC electrode towards sodiation when compared to lithiation, which was demonstrated in three-electrode rate tests. For C-rates of ≈2 C and beyond, the specific capacity obtained for sodiation drops below the capacity accessible for lithiation of the hard carbon anode, which can be explained by the higher HC anode resistance. Since currently hard carbons are the most promising anode material for sodium-ion batteries (SIBs), their relatively high electrode impedance upon (de)sodiation could be another challenge for a future commercialization of SIBs apart from the lower energy density and/or reduced cycling performance with respect to state-of-the-art lithium-ion batteries.

for providing the hard carbon samples from Kuraray as well as Bharat Suthar for his advice on EIS fitting.

ORCID

Fabian Linsenmann ⓘ https://orcid.org/0000-0001-8788-2584
Hubert A. Gasteiger ⓘ https://orcid.org/0000-0001-8199-8703

References

1. J. R. Dahn, *Phys. Rev. B*, **44** (1991).
2. J. Asenbauer, T. Eisenmann, M. Kuenzel, A. Kazzazi, Z. Chen, and D. Bresser, *Sustain. Energy Fuels*, 1 (2020).
3. G. E. Blomgren, *J. Electrochem. Soc.*, **164**, A5019 (2017).
4. Y. Nishi, *J. Power Sources*, **100**, 101 (2001).
5. Y. Nishi, *Interface Mag.*, **25**, 71 (2016).
6. P. Kurzweil and J. Garche, *Overview of Batteries for Future Automobiles* (Elsevier B.V) (2017).
7. R. E. Franklin, *Proc. R. Soc. A Math. Phys. Eng. Sci.*, **209**, 196 (1951).
8. M. Winter, G. H. Wrodnigg, J. O. Besenhard, W. Biberacher, and P. Novák, *J. Electrochem. Soc.*, **147**, 2427 (2002).
9. M. Winter and J. O. Besenhard, *Handb. Batter. Mater.*, 383 (2007).
10. V. Agubra and J. Fergus, *Materials (Basel).*, **6**, 1310 (2013).
11. A. J. Smith, J. C. Burns, X. Zhao, D. Xiong, and J. R. Dahn, *J. Electrochem. Soc.*, **158**, A447 (2011).
12. Encyclopedia of Electrochemical Power Sources, "Secondary batteries - Lithium rechargeable systems- Lithium ion." *Negative Electrodes: Graphite* (2009).
13. T. Zheng, Y. Liu, E. W. Fuller, S. Tseng, U. von Sacken, and J. R. Dahn, *J. Electrochem. Soc.*, **142** (1995).
14. H. Buqa, D. Goers, M. Holzapfel, M. E. Spahr, and P. Novák, *J. Electrochem. Soc.*, **152**, A474 (2005).
15. H. Buqa, M. Holzapfel, F. Krumeich, C. Veit, and P. Novák, *J. Power Sources*, **161**, 617 (2006).
16. R. Fong, U. von Sacken, and J. R. Dahn, *J. Electrochem. Soc.*, **137**, 2009 (1990).
17. D. A. Stevens and J. R. Dahn, *J. Electrochem. Soc.*, **148**, A803 (2001).
18. M. Endo, C. Kim, K. Nishimura, T. Fujino, and K. Miyashita, *Carbon N. Y.*, **38**, 183 (2000).
19. K. Tatsumi, T. Kawamura, S. Higuchi, T. Hosotubo, H. Nakajima, and Y. Sawada, *J. Power Sources*, **68**, 263 (1997).
20. H. Azuma, H. Imoto, S. N. I. Yamada, and K. Sekai, *J. Power Sources*, **81–82**, 1 (1999).
21. S. Flandrois and B. Simon, *Carbon N. Y.*, **37**, 165 (1999).
22. Y. Liu, J. S. Xue, T. Zhen, and J. R. Dahn, *Carbon N. Y.*, **34**, 193 (1996).
23. K. Sato, M. Noguchi, A. Demachi, N. Oki, and M. Endo, *Science*, **264**, 556 (1994).
24. P. Novak, D. Goers, and M. E. Spahr, *Carbons for Electrochemical Energy Storage and Conversion Systems*, ed. F. Beguin and E. Frackowiak (Crc Press) Chap. 7, p. 263 (2009).
25. B. Jache and P. Adelhelm, *Angew. Chemie - Int. Ed.*, **53**, 10169 (2014).
26. K. Nobuhara, H. Nakayama, M. Nose, S. Nakanishi, and H. Iba, *J. Power Sources*, **243**, 585 (2013).
27. P. Ge and M. Fouletier, *Solid State Ionics*, **28–30**, 1172 (1988).
28. M. M. Doeff, Y. Ma, S. J. Visco, and L. C. De Jonghe, *J. Electrochem. Soc.*, **140**, 169 (1993).
29. D. Saurel, B. Orayech, B. Xiao, D. Carriazo, X. Li, and T. Rojo, *Adv. Energy Mater.*, **8**, 1 (2018).
30. D. A. Stevens and J. R. Dahn, *J. Electrochem. Soc.*, **147**, 1271 (2002).
31. S. Komaba, W. Murata, T. Ishikawa, N. Yabuuchi, T. Ozeki, T. Nakayama, A. Ogata, K. Gotoh, and K. Fujiwara, *Adv. Funct. Mater.*, **21**, 3859 (2011).
32. K. Gotoh, M. Maeda, A. Nagai, A. Goto, M. Tansho, K. Hashi, T. Shimizu, and H. Ishida, *J. Power Sources*, **162**, 1322 (2006).
33. M. Letellier, F. Chevallier, F. Béguin, E. Frackowiak, and J. N. Rouzaud, *J. Phys. Chem. Solids*, **65**, 245 (2004).
34. J. M. Stratford, P. K. Allan, O. Pecher, P. A. Chater, and C. P. Grey, *Chem. Commun.*, **52**, 12430 (2016).
35. R. Morita et al., *J. Mater. Chem. A*, **4**, 13183 (2016).
36. S. Solchenbach, D. Pritzl, E. Jia, Y. Kong, J. Landesfeind, and H. A. Gasteiger, *J. Electrochem. Soc.*, **163**, 2265 (2016).
37. F. Linsenmann, D. Pritzl, and H. A. Gasteiger, *J. Electrochem. Soc.*, **166**, A3668 (2019).
38. R. Petibon, C. P. Aiken, N. N. Sinha, J. C. Burns, H. Ye, C. M. VanElzen, G. Jain, S. Trussler, and J. R. Dahn, *J. Electrochem. Soc.*, **160**, A117 (2013).
39. R. Morasch, B. Suthar, and H. A. Gasteiger, *J. Electrochem. Soc.*, **167**, 100540 (2020).
40. S. Solchenbach, D. Pritzl, E. J. Y. Kong, J. Landesfeind, and H. A. Gasteiger, *J. Electrochem. Soc.*, **163**, A2265 (2016).
41. K. G. Gallagher et al., *J. Electrochem. Soc.*, **163**, A138 (2016).
42. J. Landesfeind, D. Pritzl, and H. A. Gasteiger, *J. Electrochem. Soc.*, **164**, A1773 (2017).
43. S. Solchenbach, *PhD Thesis*, Technical University of Munich (2018).
44. J. Y. Song, H. H. Lee, Y. Y. Wang, and C. C. Wan, *J. Power Sources*, **111**, 255 (2002).
45. S. Oswald, D. Pritzl, M. Wetjen, and H. A. Gasteiger, *J. Electrochem. Soc.*, **167**, 100511 (2020).
46. C. Bommier, W. Luo, W. Y. Gao, A. Greaney, S. Ma, and X. Ji, *Carbon N. Y.*, **76**, 165 (2014).
47. M. Dollé, F. Orsini, A. S. Gozdz, and J.-M. Tarascon, *J. Electrochem. Soc.*, **148**, A851 (2002).
48. E. Barsoukov, J. H. Kim, C. O. Yoon, and H. Lee, *J. Electrochem. Soc.*, **145**, 2711 (2006).
49. J. Yao, G. X. Wang, J. H. Ahn, H. K. Liu, and S. X. Dou, *J. Power Sources*, **114**, 292 (2003).
50. N. Paul, J. Wandt, S. Seidlmayer, S. Schebesta, M. J. Mühlbauer, O. Dolotko, H. A. Gasteiger, and R. Gilles, *J. Power Sources*, **345**, 85 (2017).
51. F. M. Courtel, S. Niketic, D. Duguay, Y. Abu-Lebdeh, and I. J. Davidson, *J. Power Sources*, **196**, 2128 (2011).
52. J. Landesfeind, A. Eldiven, and H. A. Gasteiger, *J. Electrochem. Soc.*, **165**, A1122 (2018).
53. D. Aurbach, E. Zinigrad, H. Teller, and P. Dan, *J. Electrochem. Soc.*, **147**, 1274 (2002).